Hindawi
Geofluids
Volume 2021, Article ID 5945398, 16 pages
https://doi.org/10.1155/2021/5945398

Research Article

Study on the Adsorption Effect of Renewable Biochar Based on Energy Gain

Zhanghang Yang,[1] **Qixiang Xu**,[2] **Ruiqin Zhang**,[2] **Qianming Huang**,[1] **and Mingxin Liu**[1]

[1]*College of Chemistry, Zhengzhou University, Zhengzhou 450001, China*
[2]*College of Ecology and Environment, Zhengzhou University, Zhengzhou 450001, China*

Correspondence should be addressed to Qixiang Xu; xuqixiang@zzu.edu.cn

Received 10 July 2021; Revised 14 September 2021; Accepted 28 September 2021; Published 31 October 2021

Academic Editor: Xudong Zhang

This paper provides sufficient evidence on how the crop-residual-derived charcoal could effectively restore the soil polluted by the heavy metal. In this paper, straw char at three temperatures of 300°C, 500°C, and 700°C, labeled as RS300, RS500, and RS700, was prepared by low temperature pyrolysis technique using straw as raw material, and the competitive adsorption desorption of Pb^{2+}, Cd^{2+}, Cu^{2+}, and Zn^{2+} in acidic solution and the mechanism were investigated by static adsorption experiments. Since the crop-residual-derived charcoal could effectively restore the nutritional structure of the soil, which contributes to preventing the decrease in grain yield, and it is also a kind of renewable environment-friendly resource by itself, which could be used in control the pollution of heavy metal ions, it is expected that the crop-residual-derived charcoal will be a new adsorption material that could be used to control the heavy metal pollution in the future; the adsorption effect of biochar as new adsorption material on heavy metal ions has a distinct advantage over traditional adsorbent materials, and biochar is a renewable energy source, which is cheap and better for recycling resources.

1. Introduction

As the rapid development of economy, the progress of urbanization and industrialization is getting faster and faster nowadays. A large amount of heavy metal like zinc, copper, cadmium, lead, and mercury has been discharged into the air, water body, and soil, leading to an increasingly serious environmental problem. In our country, the arable land of approximate 180 million *mu* in area has been polluted by the heavy metals such as Pb, Cd, Cu, and Zn, and more than 10 million tons of grain is polluted by cadmium (known as Cd grain), zinc (known as Zn grain), and other heavy metals in each year, resulting in a direct economic loss of more than RMB 20 billion yuan [1]. In recent years, soil heavy metal pollution incident frequently occurs in China, which has seriously affected the quality of arable land and agricultural products and has significantly endangered the health of people and the stability of society [2]. Since the soil heavy metal pollution is also characterized with accumulation, concealment, and long-term persistence, they may not only form serious impact on the growth and yield of crops but also accumulate in animals and plants through the food chain after being discharged into the soil, resulting in a serious threat to the health of living organisms and human beings [3]. Currently, there are many ways to control soil pollution, mainly including physical, chemical, and biological methods. In general, the chemical adsorption method is considered to be the preferential option, due to its advantages such as moderate price, simple operation, and effective abatement effect. Meanwhile, charcoal, among all the chemical adsorption methods, could be taken as the adsorption material and play a huge role in treating the heavy metal pollution, taking into account that (i) its surface is rich in various functional groups, with well-developed porous structure, (ii) it has a large specific surface area, and (iii) the particle surface contains a large amount of negative charges, with a high charge density. Adding it to the soil can significantly improve the physical and chemical properties of the soil, especially the adsorption ability of heavy metals which shows good prospects. The source of charcoal is extensive. Since China is a

major rice cultivation country, the use of rice straw to produce charcoal for controlling heavy metal pollution of the soil will not only contribute to protecting the environment and turning waste into treasure but also improve the resource utilization rate. Therefore, there is a far-reaching significance to carry out the study on treatment of soil heavy metal pollution to improve the quality of agricultural products and protect the people's health. Currently, the problem of heavy metal pollution has attracted wide attention in the world, which has been taken as the focus and direction by many environmentalists in their research activities [4, 5].

Soil is one of the major natural resources on which mankind lives, and it is also the material basis for human and other animals to get food and extract nutrients. However, with the development of mining, smelting, and electroplating industries in recent years, soil heavy metal pollution has become increasingly serious, especially the pollution of arable land by heavy metals, which has been considered as one of the major factors impacting the food safety of our country and has attracted extensive attention [6]. Currently, heavy metal pollution of the soil is gradually increasing in China, the area of which has expanded year by year, with the source showing a trend of diversified development. As it is revealed by the statistical data, about 30 billion to 40 billion tons of untreated industrial waste water is discharged in China per year, which is used to irrigate the farmland that accounts for more than 45% of the total area of farmland irrigated with waste water in our country [7]. By the end of 2011, the arable land of about 20 million *mu* in area has been polluted by the heavy metal such as Cd, Pb, As, Cr, Cu, and Zn, which accounts for one-fifth of the total area of the arable land in China. About 12 million tons of grain is polluted by the heavy metal per year. Since the heavy metal contaminants in the acidic soil are characterized with poor mobility and long persistence and could not be easily degraded by soil microorganisms, it is very difficult to carry out the subsequent treatment work after the soil has been polluted by heavy metals. Therefore, it is urgent to conduct the prevention and control of soil heavy metal pollution.

Heavy metal pollution of the soil will affect the growth and development of plants at first, then the yield and quality of agricultural products. In the field crops, the major heavy metal contaminants to China's agricultural products include Pb, Cd, Cu, and Zn [8, 9]. Heavy metals migrate actively in the environment; as a kind of chemical elements with comparatively severe toxicity to organisms and human beings, they are absorbed by human mainly through the chain soil–crops–food. It is shown in the studies that more than 70% of Pb, Cd, Cu, Zn, and other heavy metal elements in the human body derive from the food and vegetables [10, 11]. Heavy metal pollution of the soil could lead to reduction in yield and quality of agricultural products, significantly affecting the sustainable development of the agriculture in our country, which could further threaten the life and health of human through accumulation in the food chain [12]. Cadmium, for example, could combine with mercaptan amino acids and proteins, leading to inactivation of amino acid protein, even leading to death of the plant; cadmium could also affect the activity of antioxidant enzymes in plants, destruct the cell membrane system and biological macromolecules such as protein through generating excessive oxygen free radicals, thus could inhibit the synthesis of rice chlorophyll and the growth of plant. If a person consumes cadmium-contaminated food for a long time, his renal tubular function will be affected, and the person will be susceptible to the cartilage disease. Lead has great harm to human bone marrow hematopoietic system and nervous system, which, after accumulating to a certain amount in the body, will damage the function of the kidneys and the intelligence. Long-term consumption of lead-contaminated food will also cause high teratogenic and carcinogenic risk. Heavy metal pollution of the soil also brings serious economic loss to the country. It is reported that the heavy metal pollution causes a grain yield reduction of more than 10 million tons every year, and about 12 million tons of grain is polluted by heavy metals in each year. Therefore, the heavy metal pollution could cause a total economic loss of at least RMB 20 billion yuan.

The traditional activated carbon uses coal as raw material, and the raw coal contains a certain amount of silicon-aluminum oxide [13], and the ash content is generally high. Therefore, the formation of coal-based activated carbon pore structure is limited. While coal is a nonrenewable energy source, the raw material of biomass activated carbon is agricultural and forestry waste, such as jujube [14, 15], walnut shell [16], walnut shell [17], tea-leaf waste [18, 19], corn cob [20, 21], coconut shell [22, 23], beetroot [24], peanut shell [25], rice hull [13], cotton shell [20], banana peel [20], bamboo waste [26], olive nucleus [27], cherry nucleus [28], orange peel [29], coffee bean pod [30], corn stover [31], and cassava skin [32]. They are rich in source and low in price as well as renewable. What is more, activated carbon based on biomass realizes the reusing of waste resource. So, in recent years, the preparation and application of biomass activated carbon have attracted much attention. Moreover, compared with traditional adsorption materials, biomass activated carbon has the advantages of large specific surface area, large adsorption capacity, fast adsorption speed, mild desorption conditions, and easy regeneration. As a new type of adsorption material, biomass activated carbon is becoming to be more widely used to treat heavy metal ions in wastewater.

2. Experiment

2.1. Experimental Equipment. All solutions are prepared by deionized water, and all reagents are made of analytical reagent. Experiment reagents include acetic acid, sodium acetate, acid, sodium hydroxide, lead nitrate, cadmium nitrate, copper nitrate, zinc nitrate, Pb standard solution (1 g/L), Cd standard solution (1 g/L), Cu standard solution (1 g/L), and Zn standard solution (1 g/L). The experimental preparation process is shown in Figure 1.

(1) *Adsorption and Desorption Background Solution, 0.02 mmol/L Acetic Acid +0.02 mmol/L Sodium Acetate, pH* = 4.5. Take 1.64 g sodium acetate (CH3COONa); add 1.15 mL glacial acetic acid

Figure 1: The experimental preparation process.

(CH3COOH, 98%); then add deionized water to dilute it up to 950 mL; measure the pH value of the solution, adjust the pH value of the solution to 4.5 with the pH regulation solution, and add deionized water to a specified volume

(2) *Heavy Metal Ion Mother Solution*. $Cu(NO_3)_2$ solution with a concentration of 1 mmol/L is used to prepare 1000 mL mother solution, diluted by the deionized water to a specified volume to get the copper ion mother solution. Preparation of zinc, cadmium, and lead ion mother solutions adopts the same process as that for preparing the copper ion mother solution

(3) *Heavy Metal Ions Mixed Operating Solution*. Put the background solution (pH = 4.5) for 4 heavy metal ions and mother solutions of heavy metal ions at different volumes into 7 volumetric flasks of 1000 mL, to prepare heavy metal ions mixed operating solutions with 7 gradient concentrations, i.e., 0 (background solution, pH = 4.5), 0.1, 0.5, 1.0, 2.5, 5.0, and 10.0 mmol/kg

(4) *pH Regulation Solution*. NaOH or HCl solution with the concentration of 0.1 mol/L

(5) *Preparation of Mixed Standard Solutions*. It adopts the same preparation method as that for preparing the mixed operating solutions, and the concentrations for 4 metal ions are listed as below

Standard curve range of Cu concentration measured by Atomic Absorption Spectroscopy (AAS): 0.0, 0.1, 0.5, 1, and 5 mg/L

Standard curve range of Zn concentration measured by Atomic Absorption Spectroscopy (AAS): 0.0, 0.1, 0.5, 1, and 2 mg/L

Standard curve range of Cd concentration measured by Atomic Absorption Spectroscopy (AAS): 0.0, 0.1, 0.5, 1, and 2 mg/L

Standard curve range of Cd concentration measured by Atomic Absorption Spectroscopy (AAS): 0.0, 0.1, 1.0, 5, and 10 mg/L

Equipment used in the experiment includes table top high-speed centrifuge, Atomic Absorption Spectroscopy, electronic balance, pH meter, ultrapure water device, chamber-type resistance furnace, constant-temperature water bath oscillator, and Fourier transform infrared spectrometer, detailed in Table 1.

2.2. Preparation Method and Process of Crop-Residual-Derived Charcoal. For charring, weigh certain an amount of air dried crop stalks, which are pyrolyzed under a condition isolated from oxygen, at 300°C, 500°C, and 700°C, respectively [33]. The detailed steps are listed below. Put the beaker into the muffle furnace for charring (at a temperature increasing speed rate of 10°C/min, up to 300°C ~700°C); raise the temperature to the specified level and keep for 2 hours; open the door of furnace slightly and let the beaker cool down to the ambient temperature, and take the beaker out and weigh. The same process is adopted to prepare about 100 g charcoal at each temperature level; and after being ground and screened at 60 mesh, the charcoal is stored properly.

For selection, only charcoal produced at 300°C, 500°C, and 700°C could be selected as the adsorbing material in the experiment, identified as RS300, RS500, and RS700, respectively.

2.3. Experimental Methods. The experiment is composed of two parts, and the sample size for each part is calculated as below: 7 blank control samples without addition of any adsorbing material (i.e., working solution with a concentration of 0 ~ 2.5 mmol/L, no repetition) +3 processing samples (charcoal BC300, BC500, and BC700 prepared at 300°C, 500°C, and 700°C, respectively) ×7 working solutions ×2 repetitive times =49 samples.

2.3.1. Competitive Adsorption Experiment

(1) *Weighing*. To weigh the charcoal samples with a centrifuge tube of 50 mL in accordance with the requirements specified in the table above

(2) *Solution Addition*. To move 25 mL heavy metal ion working solution (copper ion solution, 0 ~ 2.5 mmol/L) accurately with a pipette of 25 mL

(3) *Vibration*. To horizontally place and vibrate the solution at a rate of 220 r/min at 25°C for 24 hours

(4) *Centrifuging*. To centrifuge the solution at a rate of 4000 r/min for 10 minutes

(5) *Filtering*. To filter the solution with the quantitative filter paper, to measure the pH value of the filtered solution after it has been shaken evenly, and to add 1 drop of concentrated nitric acid and shake it evenly

(6) *Measurement*. To measure the concentration of heavy metal ions in the filtered solution with the Atomic Absorption Spectroscopy (AAS)

2.3.2. Competitive Desorption Experiment

(1) *Drying*. To put the centrifuge tube (including residuals) that has been centrifuged in the adsorption

Table 1: Experimental equipment.

Name	Type
Desktop high speed centrifuge	TG20-WS
Atomic absorption spectrophotometer	AA-6300CF
Electronic balance	ME104E/02
pH meter	PHS-3C
Ultrapure water machine	UPW-20N
Box type resistance furnace	SX2-10-12
Constant temperature water bath oscillator	SHA-BA
Fourier transform infrared spectrometer	NICOLET iS10

experiment into the drying chamber and to dry it up to a constant weight at 45°C

(2) *Solution Addition*. To move 25 mL adsorption and desorption background solution (acetic acid of 0.02 mol/L + sodium acetate of 0.02 mol/L, pH = 4.5) accurately with a pipette of 25 mL

(3) *Vibration*. To horizontally place and vibrate the solution at a rate of 220 r/min at 25°C for 24 hours

(4) *Centrifuging*. To centrifuge the solution at a rate of 4000 r/min for 10 minutes

(5) *Filtering*. To filter the solution with the quantitative filter paper and to add 1 drop of concentrated nitric acid and shake it evenly

(6) *Measurement*. To measure the concentration of heavy metal ions in the filtered solution with the Atomic Absorption Spectroscopy (AAS)

3. Results and Analysis

3.1. Competitive Adsorption and Desorption of Pb^{2+} by Crop-Residual-Derived Charcoal in Acidic Solution

3.1.1. Competitive Adsorption of Pb2+ by Crop-Residual-Derived Charcoal in Acidic Solution. As it is shown in Figures 2 and 3, the adsorption of Pb^{2+} by crop-residual-derived charcoal in acidic solution is affected by the concentration of heavy metal ion. In the range of concentration for the experiment, since the amount of Pb^{2+} adsorbed by RS300, RS500, and RS700 increases as the concentration of Pb2+ increases, when the concentration of heavy metal ion reaches 2.5000 mmol/L, the amount of Pb^{2+} adsorbed by RS300, RS500, and RS700 reaches the maximum level, i.e., 410.20 mmol/kg, 393.77 mmol/kg, and 371.16 mmol/kg, respectively. The competitive adsorption rates of RS300, RS500, and RS700 show no significant variation as the concentration Pb^{2+} of increases, being kept in the range of 65% ~75%. When the concentration of heavy metal ion reaches 2.5000 mmol/L, the competitive Pb^{2+} adsorption rates of RS300, RS500, and RS700 are 66.4%, 60.0%, and 59.5%, respectively. It is suggested that the concentration of heavy metal ion has a minor effect on the Pb^{2+} adsorption capacities of three types of crop-residual-derived charcoal,

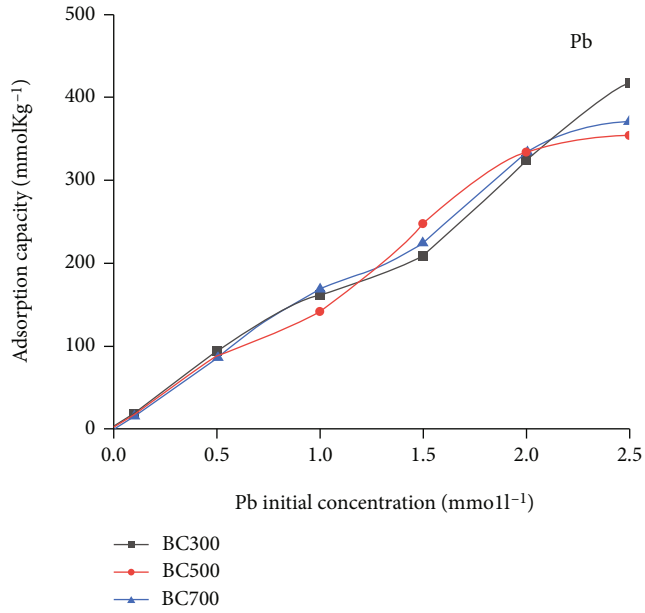

Figure 2: Adsorption rate of Pb^{2+} in straw with different concentrations of heavy metal ions.

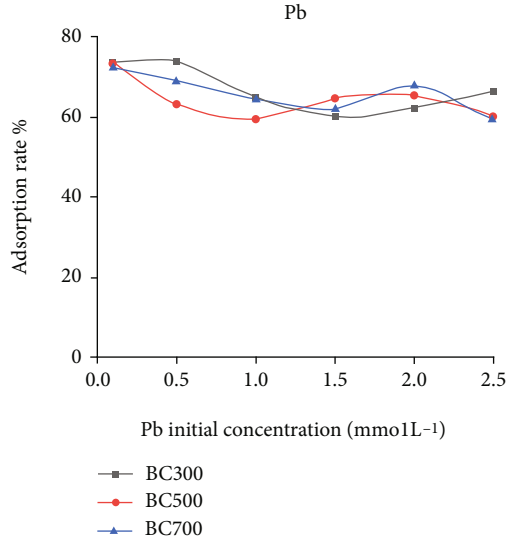

Figure 3: The adsorption rate of Pb^{2+} in the mixed working solution of straw in different concentrations of heavy metal ions.

and that when the concentration of heavy metal ion reaches 2.5000 mmol/L, RS300 shows the best effectiveness in competitive adsorption of Pb^{2+}.

3.1.2. Competitive Desorption of Pb^{2+} by Crop-Residual-Derived Charcoal in Acidic Solution. As it is shown in Figure 4, the concentration of heavy metal ion has a minor effect on the Pb^{2+} desorption rate of crop-residual-derived charcoal in acidic solution. In the range of concentration for the experiment, the desorption rate of RS300, RS500, and RS700 is kept at a low level when the concentration of Pb^{2+} increases. When the concentration of heavy metal ion

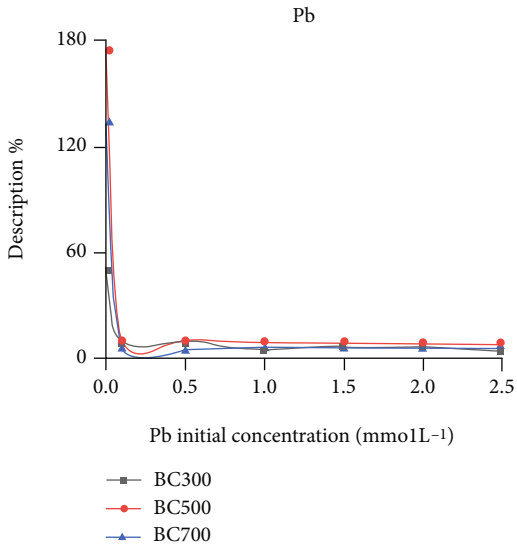

Figure 4: Desorption rate of Pb^{2+} in straw with different concentrations of heavy metal ions.

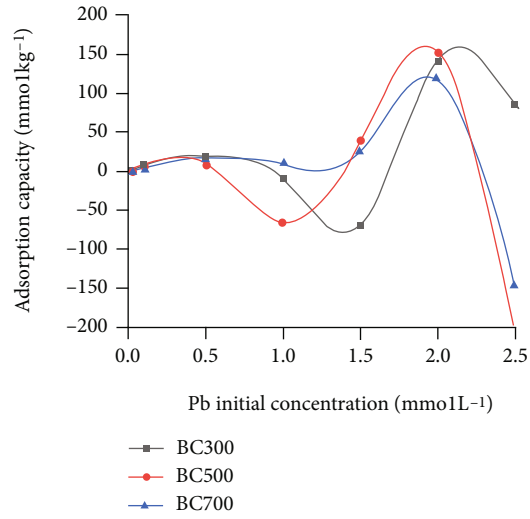

Figure 5: Adsorption of Cd^{2+} in straw with different concentrations of heavy metal ions.

reaches 2.5000 mmol/L, the competitive Pb^{2+} desorption rates of RS300, RS500, and RS700 are 7.91%, 8.05%, and 5.35%, respectively. It is suggested that the adsorption of Pb^{2+} in the acidic solution by the crop-residual-derived charcoal is very stable, and the heavy metal ion could not be desorbed easily. Therefore, it is determined that the charcoal RS300 is most effective in adsorbing Pb^{2+} when the concentration of heavy metal ion is 2.5000 mmol/L, taking into account of the results from both the competitive adsorption experiment and the competitive desorption experiment.

3.2. Competitive Adsorption and Desorption of Cd^{2+} by Crop-Residual-Derived Charcoal in Acidic Solution

3.2.1. Competitive Adsorption of Cd^{2+} by Crop-Residual-Derived Charcoal in Acidic Solution. As it is shown in Figures 5 and 6, the adsorption of Cd^{2+} by crop-residual-derived charcoal in acidic solution is affected by the concentration of heavy metal ion. In the range of concentration for the experiment, the Cd^{2+} adsorption amount and adsorption rate of RS300, RS500, and RS700 decrease firstly and increase then, and when the concentration of heavy metal ion reaches 2.000 mmol/L, the Cd^{2+} adsorption amount and adsorption rate reach the peak point. The maximum competitive adsorption amounts of RS300, RS500, and RS700 are 141.79 mmol/kg, 151.61 mmol/kg, and 117.41 mmol/kg, respectively, and the maximum competitive adsorption rates are 14.2%, 21.6%, and 27.3%, respectively. When the concentration of heavy metal ion is 1.000 mmol/L, 1.500 mmol/L, and 2.500 mmol/L, the adsorption amount and adsorption rate are low. It is suggested that the concentration of heavy metal ion has a significant effect on the competitive Cd^{2+} adsorption capacities of three types of crop-residual-derived charcoal, and that when the concentration of heavy metal ion reaches 2.0000 mmol/L, RS500 shows the best effectiveness in competitive adsorption of Cd^{2+}.

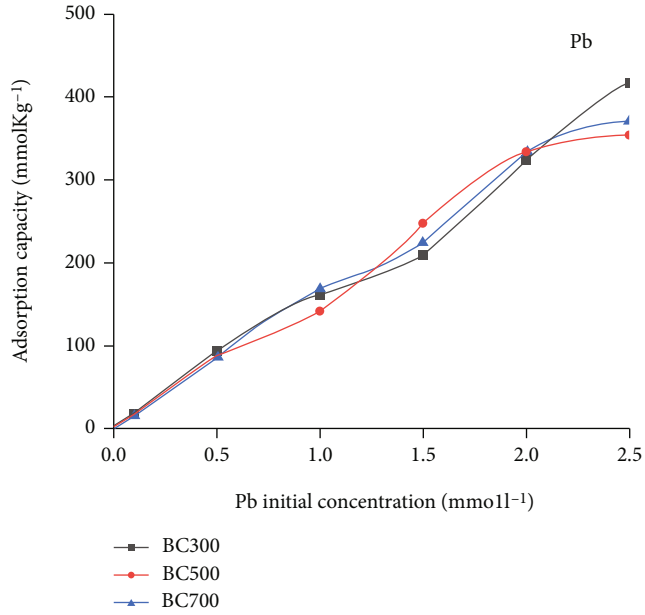

Figure 6: Adsorption rate of paddy carbon on Cd^{2+} in different concentrations of heavy metal ions in mixed working fluid.

3.2.2. Competitive Desorption of Cd^{2+} by Crop-Residual-Derived Charcoal in Acidic Solution. As it is shown in Figure 7, the competitive Cd^{2+} desorption rate of crop-residual-derived charcoal in acidic solution is affected by the concentration of heavy metal ion. In the range of concentration for the experiment, as the concentration of Cd^{2+} increases, the Cd^{2+} desorption rate of RS300 decreases firstly and increases then, and when the concentration of heavy metal ion reaches 2.000 mmol/L, the Cd^{2+} desorption rate reaches the peak point, i.e., 364.27%; the Cd^{2+} desorption rate of RS500 decreases firstly and increases then, and when the concentration of heavy metal ion reaches 1.5000 mmol/L, the Cd^{2+} desorption rate reaches the peak point, i.e., 70.26%;

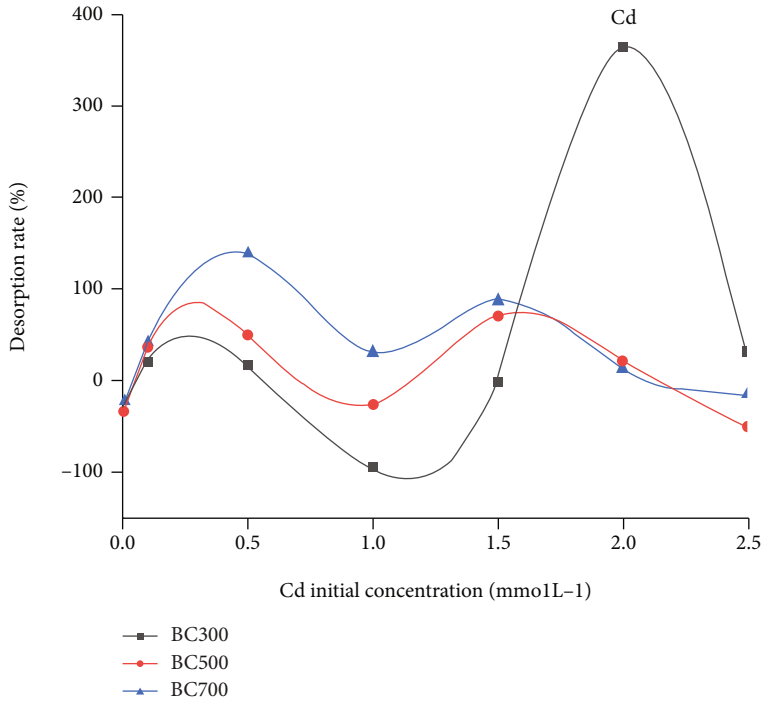

Figure 7: Desorption rate of Cd^{2+} in straws with different concentrations of heavy metal ions.

and the Cd^{2+} desorption rate of RS700 increases firstly and decreases then, and when the concentration of heavy metal ion reaches 0.5000 mmol/L, the Cd^{2+} desorption rate reaches the peak point, i.e., 138.47%. When the concentration of heavy metal ion reaches 2.000 mmol/L and 2.5000 mmol/L, the competitive Pb^{2+} desorption rates of RS500 and RS700 are very low. It is suggested that the adsorption of Cd^{2+} in the acidic solution by the crop-residual-derived charcoal RS500 and RS700 is very stable, and the heavy metal ion could not be desorbed easily. However, the desorption rate of RS300 is high, suggesting a poor adsorption stability. Therefore, it is determined that the charcoal RS500 is most effective in adsorbing Cd^{2+} when the concentration of heavy metal ion is 2.0000 mmol/L, taking into account the results from both the competitive adsorption experiment and the competitive desorption experiment.

3.3. Competitive Adsorption and Desorption of Cu^{2+} by Crop-Residual-Derived Charcoal in Acidic Solution

3.3.1. Competitive Adsorption of Cu^{2+} by Crop-Residual-Derived Charcoal in Acidic Solution. As it is shown in Figures 8 and 9, the competitive adsorption of Cu^{2+} by crop-residual-derived charcoal in acidic solution is affected by the concentration of heavy metal ion. In the range of concentration for the experiment, as the concentration of Cu^{2+} increases, the Cu^{2+} adsorption amount of RS300, RS500, and RS700 increases, and the Cu^{2+} adsorption rate keeps steady firstly and increases then, and when the concentration of heavy metal ion reaches 2.000 mmol/L, the Cd^{2+} adsorption amount and adsorption rate reach the peak point. The maximum competitive adsorption amounts of RS300, RS500, and RS700 are 103.53 mmol/kg, 264.04 mmol/kg, and 327.77 mmol/kg, respectively, and the maximum competitive adsorption rates are 29.13%, 50.0%, and 73.5%, respectively. When the concentration of heavy metal ion is 2.500 mmol/L, the adsorption amount and adsorption rate of all these three types of crop-residual-derived charcoal are low. It is suggested that the concentration of heavy metal ion has a minor effect on the competitive Cu^{2+} adsorption capacities of three types of crop-residual-derived charcoal, and that when the concentration of heavy metal ion reaches 2.0000 mmol/L, RS700 shows the best effectiveness in competitive adsorption of Cu^{2+}.

3.3.2. Competitive Desorption of Cu^{2+} by Crop-Residual-Derived Charcoal in Acidic Solution. As it is shown in Figure 10, the competitive Cu^{2+} desorption rate of crop-residual-derived charcoal in acidic solution is affected by the concentration of heavy metal ion. In the range of concentration for the experiment, as the concentration of Cu^{2+} increases, the Cu^{2+} desorption rate of RS300 increases firstly and decreases then, and when the concentration of heavy metal ion reaches 1.000 mmol/L, the Cu^{2+} desorption rate reaches the peak point, i.e., 436.80%; and the Cu^{2+} desorption rate of RS500 shows no significant variation. It is suggested that the adsorption of Cu^{2+} in the acidic solution by the crop-residual-derived charcoal RS500 and RS700 is very stable, and the heavy metal ion could not be desorbed easily. However, the desorption rate of RS300 varies significantly, suggesting a poor adsorption stability. Therefore, it is determined that the charcoal RS700 is most effective in adsorbing Cu^{2+} when the concentration of heavy metal ion is 2.0000 mmol/L, taking into account of the results from both the competitive adsorption experiment and the competitive desorption experiment.

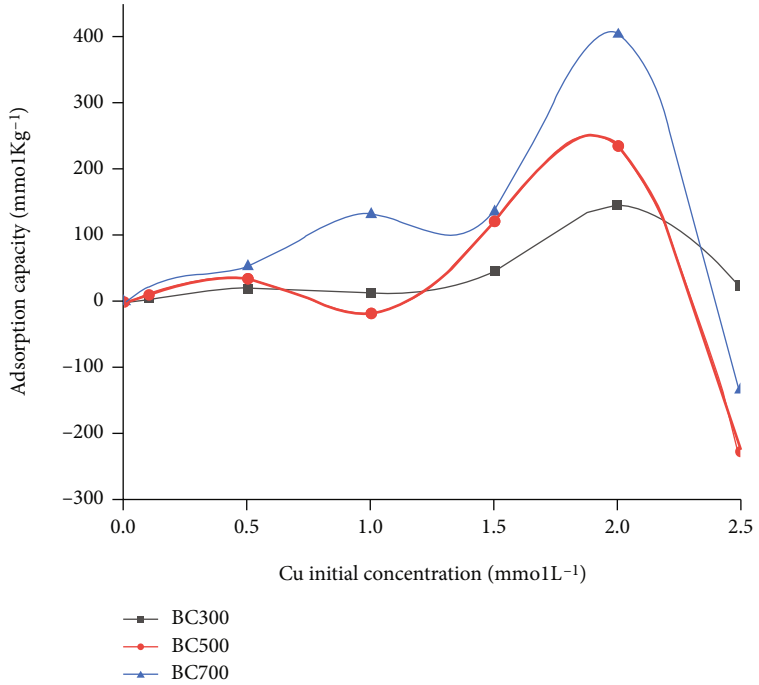

Figure 8: Adsorption of Cu^{2+} in straw with different concentrations of heavy metal ions.

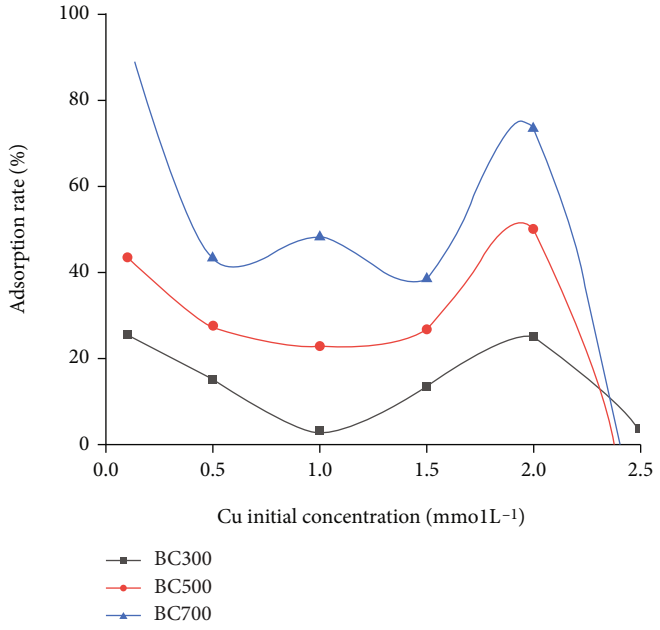

Figure 9: Adsorption rate of Pb^{2+} in straw with different concentrations of heavy metal ions.

3.4. Competitive Adsorption and Desorption of Zn^{2+} by Crop-Residual-Derived Charcoal in Acidic Solution

3.4.1. Competitive Adsorption of Zn^{2+} by Crop-Residual-Derived Charcoal in Acidic Solution. As it is shown in Figures 11 and 12, the adsorption of Zn^{2+} by crop-residual-derived charcoal in acidic solution is affected by the concentration of heavy metal ion. In the range of concentration for the experiment, the Zn^{2+} adsorption amounts of RS300, RS500, and RS700 increase firstly and decrease up to zero then, and when the concentration of heavy metal ion reaches 0.5000 mmol/L, the Zn^{2+} adsorption amount reaches the peak point. The maximum competitive adsorption amounts of RS300, RS500, and RS700 are 21.66 mmol/kg, 6.16 mmol/kg, and 8.82 mmol/kg, respectively. As the concentration of Zn^{2+} increases, the competitive adsorption rate increases

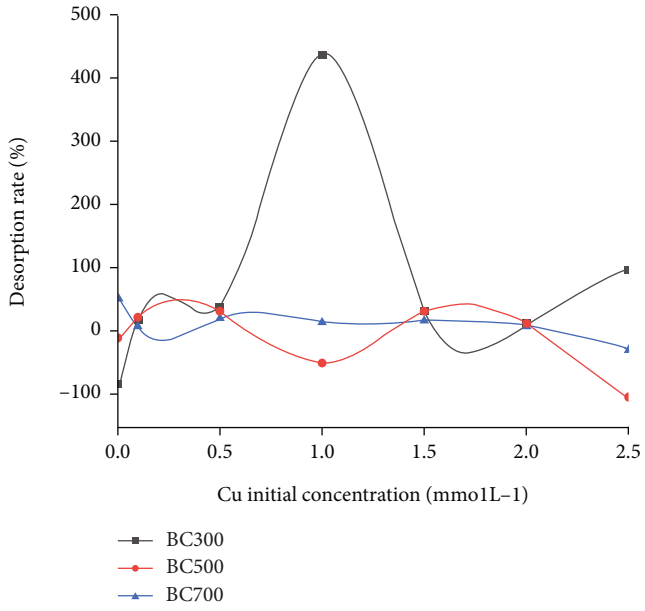

Figure 10: Desorption rate of Cu^{2+} in straw with different concentrations of heavy metal ions in mixed working fluid.

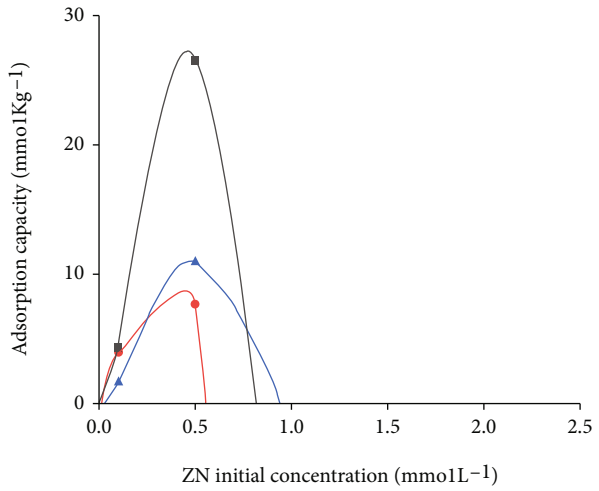

Figure 11: Adsorption of Zn^{2+} in straw with different concentrations of heavy metal ions.

firstly and decreases then. When the concentration of heavy metal ion is 2.000 mmol/L, the adsorption rates are 25.0%, 50.0%, and 73.5%, respectively. When the concentration of heavy metal ion is 2.500 mmol/L, the absorption rates of RS500 and RS700 reach the lowest level. It is suggested that the concentration of heavy metal ion has a significant effect on the competitive Zn^{2+} adsorption capacities of three types of crop-residual-derived charcoal, and that when the concentration of heavy metal ion reaches 0.5000 mmol/L, RS300 shows the best effectiveness in competitive adsorption of Zn^{2+}.

3.4.2. Competitive Desorption of Zn^{2+} by Crop-Residual-Derived Charcoal in Acidic Solution. As it is shown in

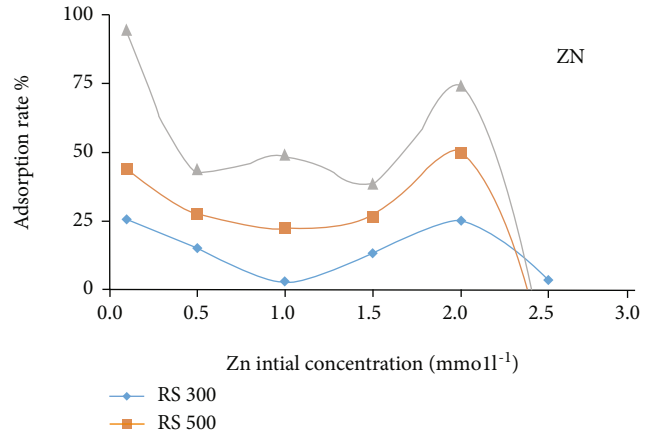

Figure 12: Adsorption of Zn^{2+} at different concentrations of heavy metal ions in mixed working fluid.

Figure 13, the competitive Zn^{2+} desorption rate of crop-residual-derived charcoal in acidic solution is affected by the concentration of heavy metal ion. In the range of concentration for the experiment, as the concentration of Zn^{2+} increases, the Zn^{2+} desorption rate of RS700 decreases firstly and approaches zero then. When the concentration of heavy metal ion reaches 2.000 mmol/L, the Zn^{2+} desorption rate reaches the peak point, i.e., 99.76%; the Zn^{2+} desorption rate of RS500 decreases firstly and reaches zero finally. It is suggested that the Zn^{2+} desorption rates of RS500 and RS700 in the acidic solution are low, while the desorption rate of RS300 varies significantly, suggesting a poor adsorption stability. Therefore, it is not recommended to realize the competitive adsorption of Zn^{2+} with the crop-residual-derived charcoal, taking into account the results from both the competitive adsorption experiment and competitive desorption experiment.

3.5. Isothermal Adsorption Model. The static adsorption capacity is an important measurement to describe and predict the adsorption performance of an adsorbent. Therefore, the Langmuir model and Freundlich model could be used to analyze the competitive adsorption properties of the crop-residual-derived charcoal in acidic solution according to the difference of sample concentration before and after adsorption [34]. In the above experiments, we set up seven groups of different heavy metal ion concentration gradient and test the concentration of heavy metal ions in the corresponding solution after the adsorption equilibrium. The obtained data are converted into the adsorption capacity. The equation of Langmuir, $C_e/q_e = C_e/q_{\max} + 1/(q_{\max}K_f)$, and the equation of Freundlich, $\ln q_e = \ln K_f + (1/n) \ln C_e$, have been used to fit the isothermal adsorption curves for Pb(II), Cd(II), Cu(II), and Zn(II). The results are shown in Tables 2–5.

3.5.1. Model for Competitive Adsorption of Pb^{2+} by Crop-Residual-Derived Charcoal in Acidic Solution. As it is shown in Table 2, the competitive adsorption model of Pb^{2+} by three types of crop-residual-derived charcoal (RS300,

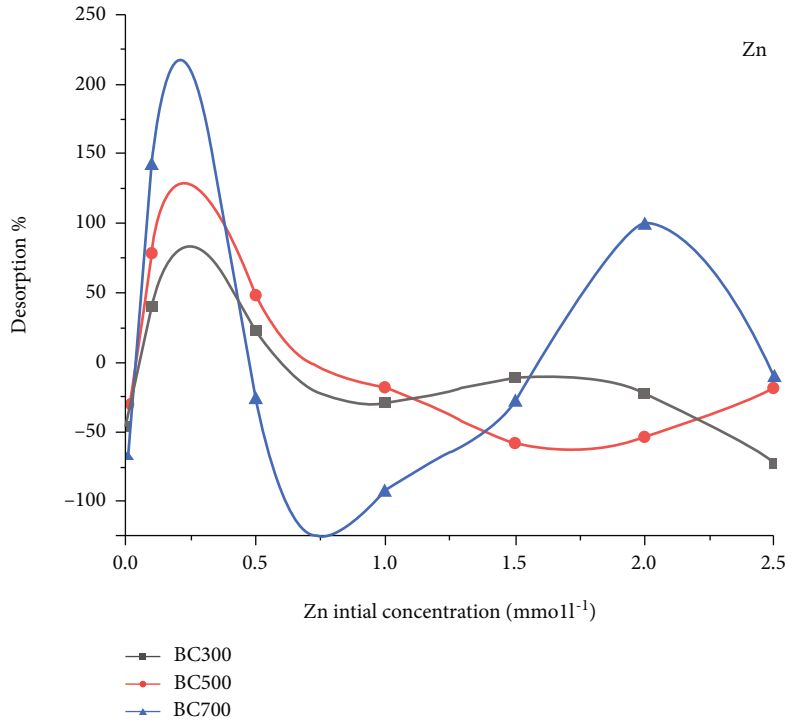

Figure 13: Desorption rate of Zn^{2+} in straw with different concentrations of heavy metal ions.

Table 2: Competitive adsorption model of Pb^{2+} in acid solution of straw carbon.

Adsorption model	Sample types	Linear regression equation	R^2	q_{max}	K_f	n
Langmuir	RS300	$y = 0.0012x + 0.0015$	0.595	833.3	—	—
	RS500	$y = 0.001x + 0.0018$	0.4481	1000.0	—	—
	RS700	$y = 0.0011x + 0.0016$	0.6953	909.1	—	—
Freundlich	RS300	$y = 0.8304x + 6.0218$	0.9807	—	412.3	1.20
	RS500	$y = 0.8434x + 5.9408$	0.9838	—	380.2	1.19
	RS700	$y = 0.8536x + 6.0024$	0.9906	—	404.4	1.17

Table 3: Competitive adsorption model of Cd^{2+} in acidic solution of straw carbon.

Adsorption model	Sample types	Linear regression equation	R^2	q_{max}	K_f	n
Langmuir	RS300	$y = -0.0572x - 0.0301$	0.2566	17.5	—	—
	RS500	$y = 0.0007x - 0.0208$	0.5073	1428.6	—	—
	RS700	$y = -0.0488x + 0.0989$	0.4490	20.5	—	—
Freundlich	RS300	$y = 0.8685x + 3.9137$	0.9532	—	8.8	1.88
	RS500	$y = 0.6515x + 4.2502$	0.9985	—	7.2	1.75
	RS700	$y = 0.3424x + 4.9728$	0.9904	—	7.9	2.19

RS500, and RS700) in acidic solution has shown a good fit to the isothermal adsorption equation of Freundlich model, and all R^2 values are more than 0.98. However, when the Langmuir model is used for fitting, it is found that the linearity is significantly inferior to that of the Freundlich model.

The Langmuir isothermal adsorption equation is used to calculate the maximum equilibrium adsorption capacities q_{max} of RS300, RS500, and RS700, which are 833.3 mmol/kg, 1000.0 mmol/kg, and 909.1 mmol/kg, respectively. They are close to the experimental data, suggesting that the adsorption

Table 4: Competitive adsorption model of Cu^{2+} in acidic solution of straw carbon.

Adsorption model	Sample types	Linear regression equation	R^2	q_{max}	K_f	n
Langmuir	RS300	$y = 0.0332x - 0.0013$	0.5778	30.1	—	—
	RS500	$y = 0.0047x + 0.0047$	0.1890	212.8	—	—
	RS700	$y = 0.0042x + 0.0017$	0.3475	238.1	—	—
Freundlich	RS300	$y = 0.0395x + 4.7604$	0.94316	—	116.80	25.32
	RS500	$y = -0.0562x + 4.5199$	0.99852	—	91.83	17.79
	RS700	$y = 0.1036x + 4.7731$	0.99039	—	118.29	9.65

Table 5: Competitive adsorption model of Zn^{2+} in acidic solution of straw carbon.

Adsorption model	Sample types	Linear regression equation	R^2	q_{max}	K_f	n
Langmuir	RS300	$y = -0.0352x + 0.0222$	0.6671	28.4	—	—
	RS500	$y = -0.0245x + 0.0236$	0.3326	40.8	—	—
	RS700	$y = -0.032x + 0.0458$	0.5577	31.3	—	—
Freundlich	RS300	$y = 0.787x + 3.5767$	0.9214	—	35.8	1.27
	RS500	$y = 0.6721x + 2.9228$	0.8968	—	18.6	1.49
	RS700	$y = 0.919x + 2.8279$	0.9682	—	16.9	1.09

of Pb^{2+} by charcoal in the acidic solution is very stable, and the adsorption stability is sequenced as RS500 > RS700 > RS300.

In the Freundlich equation, the characterization parameter K_f for adsorption capacity also shows the similar trend, further suggesting that the competitive adsorption of Pb^{2+} by three types of charcoal in the acidic solution is very stable. As it is known based on the data from the Freundlich adsorption model analysis, in the competitive adsorption of Pb^{2+} by three types of crop-residual-derived charcoal, n values are all more than 1, and it could be determined that the competitive adsorption of Pb^{2+} by the crop-residual-derived charcoal in acidic solution is in a standard Freundlich adsorption mode.

3.5.2. Model for Competitive Adsorption of Cd^{2+} by Crop-Residual-Derived Charcoal in Acidic Solution. As it is shown in Table 3, the competitive adsorption of Cd^{2+} by three types of crop-residual-derived charcoal (RS300, RS500, and RS700) in acidic solution has shown a good fit to the isothermal adsorption equation of Freundlich model, and all R^2 values are more than 0.95. However, when the Langmuir model is used for fitting, it is found that the linearity is significantly inferior to that of the Freundlich model.

The Langmuir isothermal adsorption equation is used to calculate the maximum equilibrium adsorption capacities q_{max} of RS300, RS500, and RS700, which are 17.5 mmol/kg, 1428.6 mmol/kg, and 20.5 mmol/kg, respectively. They are close to the experimental data, suggesting that the adsorption of Cd^{2+} by charcoal in the acidic solution is very stable, and the adsorption stability is sequenced as RS500 > RS 700 > RS300.

In the Freundlich equation, the characterization parameter K_f for adsorption capacity also shows the similar trend, further suggesting that the competitive adsorption of Pb^{2+} by three types of charcoal in the acidic solution is very stable. As it is known based on the data from the Freundlich adsorption model analysis, in the competitive adsorption of Cd^{2+} by three types of crop-residual-derived charcoal, n values are all more than 1, and it could be determined that the competitive adsorption of Cd^{2+} by the crop-residual-derived charcoal in acidic solution is in a standard Freundlich adsorption mode.

3.5.3. Model for Competitive Adsorption of Cu^{2+} by Crop-Residual-Derived Charcoal in Acidic Solution. As it is shown in Table 4, the competitive adsorption of Cu^{2+} by three types of crop-residual-derived charcoal (RS300, RS500, and RS700) in acidic solution has shown a good fit to the isothermal adsorption equation of Freundlich model, and all R^2 values are more than 0.94. However, when the Langmuir model is used for fitting, it is found that the linearity is significantly inferior to that of the Freundlich model.

The Langmuir isothermal adsorption equation is used to calculate the maximum equilibrium adsorption capacities q_{max} of RS300, RS500, and RS700, which are 30.1 mmol/kg, 212.8 mmol/kg, and 238.1 mmol/kg, respectively. They are close to the experimental data, suggesting that the adsorption of Cu^{2+} by charcoal in the acidic solution is very stable, and the adsorption stability is sequenced as RS700 > RS 500 > RS300.

In the Freundlich equation, the characterization parameter K_f for adsorption capacity also shows the similar trend, further suggesting that the competitive adsorption of Cu^{2+} by three types of charcoal in the acidic solution is very stable. As it is known based on the data from the Freundlich adsorption model analysis, in the competitive adsorption of Cu^{2+} by three types of crop-residual-derived charcoal, n values are all more than 1, and it could be determined that

the competitive adsorption of Cu^{2+} by the crop-residual-derived charcoal in acidic solution is in a standard Freundlich adsorption mode.

3.5.4. Model for Competitive Adsorption of Zn^{2+} by Crop-Residual-Derived Charcoal in Acidic Solution. As it is shown in Table 5, the competitive adsorption of Zn^{2+} by three types of crop-residual-derived charcoal (RS300, RS500, and RS700) in acidic solution has shown a good fit to the isothermal adsorption equation of Freundlich model, and all R^2 values are more than 0.90. However, when the Langmuir model is used for fitting, it is found that the linearity is significantly inferior to that of the Freundlich model.

The Langmuir isothermal adsorption equation is used to calculate the maximum equilibrium adsorption capacities q_{max} of RS300, RS500, and RS700, which are 28.4 mmol/kg, 40.8 mmol/kg, and 31.3 mmol/kg, respectively. They are close to the experimental data, suggesting that the competitive adsorption of Zn^{2+} by charcoal in the acidic solution is very stable, and the adsorption stability is sequenced as RS 500 > RS700 > RS300.

In the Freundlich equation, the characterization parameter K_f for adsorption capacity also shows the similar trend, further suggesting that the competitive adsorption of Zn^{2+} by three types of charcoal in the acidic solution is very stable. As it is known based on the data from the Freundlich adsorption model analysis, in the competitive adsorption of Zn^{2+} by three types of crop-residual-derived charcoal, n values are all more than 1, and it could be determined that the competitive adsorption of Zn^{2+} by the crop-residual-derived charcoal in acidic solution is in a standard Freundlich adsorption mode.

3.6. Mechanism for Competitive Adsorption of Heavy Metal Ions by Crop-Residual-Derived Charcoal in Acidic Solution. In order to study the mechanism for adsorption of heavy metal ions by crop-residual-derived charcoal in the acidic solution, RS300, RS500, and RS700 are used as the adsorbents, and heavy metal ions (Pb^{2+}, Cd^{2+}, Cu^{2+}, and Zn^{2+}) are used as the adsorbed substances. Mix three types of charcoal with the heavy metal ion working solution at a solid-liquid ratio of 1: 200, adjust the pH value of the suspension to 4.5, and put the suspension into the constant-temperature shaker to shake it for 2 hours. After it is kept at 25°C for 24 hours, separate the solid and liquid of the suspension by means of vacuum filtration. Dry a part of crop-residual-derived charcoal samples that have adsorbed heavy metal ion under the infrared lamp. The Fourier Transform Infrared Spectroscopy (FTIR) is used to measure the infrared spectrum of the heavy metal ions along or the charcoal before and after competitive adsorption, with a scanning scope of 400~4000 cm^{-1}, under the resolution of 4.0 cm^{-1}. The scan is repeated for 32 times, and results are summed up. The infrared spectrums of RS300, RS500, and RS700 before and after adsorption are shown in Figure 14 [35–37].

In order to investigate the mechanism for adsorption of Pb^{2+} by crop-residual-derived charcoal in the acidic solution, the measurements have been performed for the infrared spectrums of RS300, RS500, and RS700 before and after adsorption, in which RS300, RS500, and RS700 are used as the adsorbents, and heavy metal ions (Pb^{2+}, Cd^{2+}, Cu^{2+}, and Zn^{2+}) are used as the adsorbed substances, as shown in Figures 15–18.

3.6.1. Mechanism for Competitive Adsorption of Pb^{2+} by Crop-Residual-Derived Charcoal in Acidic Solution. In order to investigate the mechanism for adsorption of Pb^{2+} by crop-residual-derived charcoal in the acidic solution, the measurements have been performed for the infrared spectrums of RS300, RS500, and RS700 before and after adsorption, in which RS300, RS500, and RS700 are used as the adsorbents, and Pb^{2+} is used as the adsorbed substance, as shown in Figure 15.

As it is shown in Figure 15, RS300 has an adsorption peak at 3,438 cm^{-1}, which is O-H stretching vibration or hydroxyl oxygen, and after adsorption of Pb^{2+}, the adsorption peak transfers to 3,408 cm^{-1} through blue shift. The adsorption peak of RS300 at 2,919 cm^{-1} is C-H stretching vibration, and after adsorption of Pb^{2+}, the adsorption peak transfers to 2,936 cm^{-1} through red shift. It suggests that hydrogen bond structure is formed by Pb^{2+} and RS300. The adsorption peak at 1,606 cm^{-1} is an adsorption peak with benzene ring framework, suggesting that it contains benzene ring-like substances. After adsorption of Pb^{2+}, the adsorption peak transfers to 1,643 cm^{-1} through red shift, suggesting that a π-π conjugated structure exists among the aromatic structure formed by Pb^{2+} and RS300. Additionally, RS300 also contains CO single bond stretching vibration (1,096 cm^{-1}) and O-Si-O bond bending vibration (1,096 cm^{-1}), and after adsorption, the adsorption peak transfers to 1,061 cm^{-1} through blue shift.

RS500 has an adsorption peak at 3,417 cm^{-1}, which is O-H stretching vibration or hydroxyl oxygen, and after adsorption of Pb^{2+}, the adsorption peak transfers to 3,408 cm^{-1} through blue shift. The adsorption peak of RS500 at 2,951 cm^{-1} is C-H stretching vibration, but after adsorption of Pb^{2+}, the adsorption peak does not shift significantly, suggesting that the functional group is not involved in the adsorption of Pb^{2+}. The adsorption peak at 1,629 cm^{-1} is an adsorption peak with benzene ring framework, suggesting that it contains benzene ring-like substances. After adsorption of Pb^{2+}, the adsorption peak transfers to 1,619 cm^{-1} through red shift, suggesting that a π-π conjugated structure exists among the aromatic structure formed by Pb^{2+} and RS500. Additionally, RS500 also contains CO single bond stretching vibration (1,104 cm^{-1}) and O-Si-O bond bending vibration (1,104 cm^{-1}), but after adsorption, these adsorption peaks do not shift significantly, suggesting that these functional groups are not involved in the adsorption of Pb^{2+}.

Similarly, RS700 has an adsorption peak at 3,417 cm^{-1}, which is O-H stretching vibration or hydroxyl oxygen, and after adsorption of Pb^{2+}, the adsorption peak transfers to 3,408 cm^{-1} through blue shift. The adsorption peak of RS700 at 2,951 cm^{-1} is C-H stretching vibration, but after adsorption of Pb^{2+}, the adsorption peak does not shift significantly, suggesting that the functional group is not involved in the adsorption of Pb^{2+}. The adsorption peak at 1,629 cm^{-1} is an adsorption peak with benzene ring framework, suggesting that

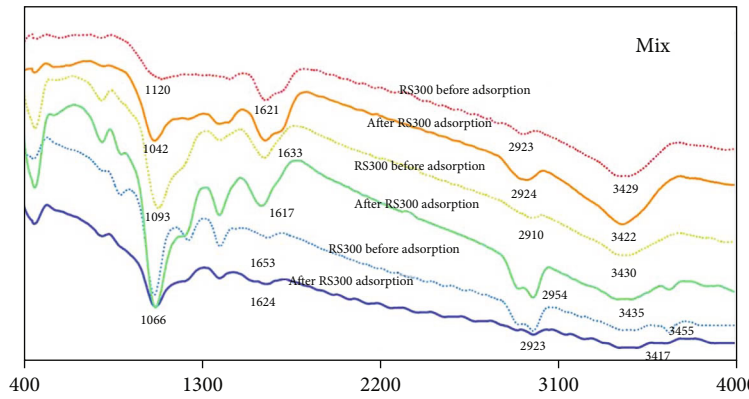

Figure 14: Adsorption mechanism of mixed metal ions in acidic solution of straw.

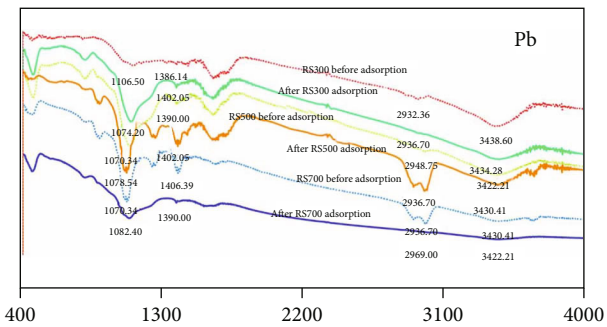

Figure 15: Competitive adsorption mechanism of Pb^{2+} in acid solution of straw.

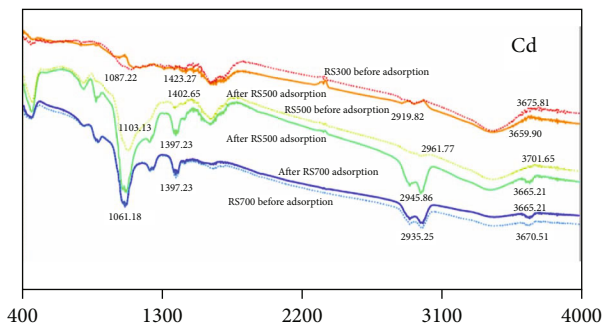

Figure 16: Competitive adsorption mechanism of cadmium on Cd^{2+} in acidic solution.

it contains benzene ring-like substances [38]. After adsorption, the adsorption peak transfers to 1,619 cm^{-1} through red shift, suggesting that a π-π conjugated structure exists among the aromatic structure formed by Pb^{2+} and RS700. Additionally, RS700 also contains CO single bond stretching vibration (1,104 cm^{-1}) and O-Si-O bond bending vibration (1,104 cm^{-1}), but after adsorption, these adsorption peaks do not shift significantly, suggesting that these functional groups are not involved in the adsorption of Pb^{2+}.

Based on data shown in Figures 14 and 15, it could be found that the mechanism of single and competitive adsorption is not different among RS300, RS500, and RS700, in which O-H stretching vibration or hydroxyl oxygen, C-H stretching vibration, benzene ring structure, and ionic effect are involved.

3.6.2. Mechanism for Competitive Adsorption of Cd^{2+} by Crop-Residual-Derived Charcoal in Acidic Solution. In order to investigate the mechanism for adsorption of Cd^{2+} by crop-residual-derived charcoal in the acidic solution, the measurements have been performed for the infrared spectrums of RS300, RS500, and RS700 before and after adsorption, in which RS300, RS500, and RS700 are used as the adsorbents, and Cd^{2+} is used as the adsorbed substance, as shown in Figure 16.

As it is shown in Figure 16, RS300 has an adsorption peak at 3,675 cm^{-1}, which is O-H stretching vibration or hydroxyl oxygen, and after adsorption of Cd^{2+}, the adsorption peak transfers to 3,659 cm^{-1} through blue shift. The adsorption peak of RS300 at 2,919 cm^{-1} is C-H stretching vibration, but after adsorption, the adsorption peak does not shift significantly, suggesting that the functional group is not involved in the adsorption. The adsorption peak at 1,423 cm^{-1} is an adsorption peak with benzene ring framework, suggesting that it contains benzene ring-like substances, but after adsorption, the adsorption peak does not shift significantly, suggesting that the functional group is not involved in the adsorption. Additionally, RS300 also contains CO single bond stretching vibration (1,087 cm^{-1}) and O-Si-O bond bending vibration (1,087 cm^{-1}), but after adsorption, the adsorption peak does not shift significantly, suggesting that these functional groups are not involved in the adsorption of Cd^{2+}.

RS500 has an adsorption peak at 3,701 cm^{-1}, which is O-H stretching vibration or hydroxyl oxygen, and after adsorption of Cd^{2+}, the adsorption peak transfers to 3,665 cm^{-1} through blue shift. The adsorption peak of RS500 at 2,961 cm^{-1} is C-H stretching vibration, and after adsorption, the adsorption peak transfers to 2,945 cm^{-1}. The adsorption peak at 1,402 cm^{-1} is an adsorption peak with benzene ring framework, suggesting that it contains benzene ring-like substances, but after adsorption, the adsorption peak does not shift significantly, suggesting that the functional group is not involved in the adsorption. Additionally, RS500 also

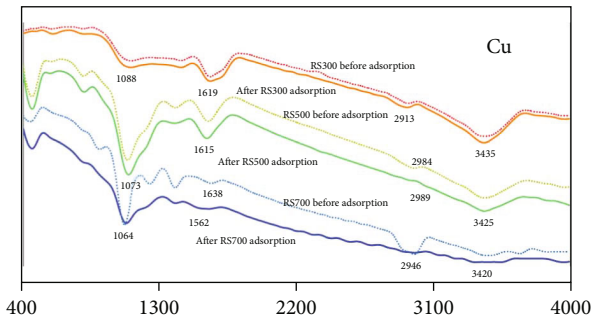

Figure 17: Competitive adsorption mechanism of Cu^{2+} in acid solution of straw.

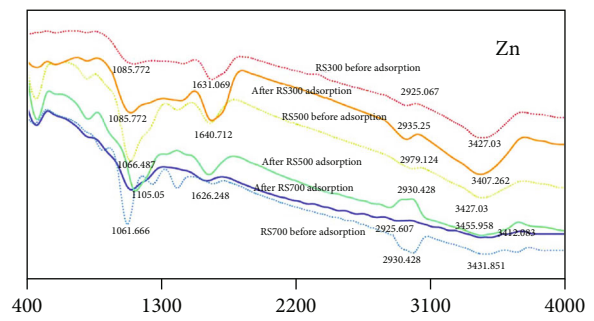

Figure 18: Competitive adsorption mechanism of Zn^{2+} in acid solution of straw.

contains CO single bond stretching vibration (1,103 cm^{-1}) and O-Si-O bond bending vibration (1,103 cm^{-1}), but after adsorption, the adsorption peak does not shift significantly, suggesting that these functional groups are not involved in the adsorption of Cd^{2+}.

Similarly, RS700 has an adsorption peak at 3,665 cm^{-1}, which is O-H stretching vibration or hydroxyl oxygen, and after adsorption of Cd^{2+}, the adsorption peak transfers to 3,670 cm^{-1} through red shift. The adsorption peak of RS500 at 2,935 cm^{-1} is C-H stretching vibration, but after adsorption, the adsorption peak does not shift significantly, suggesting that the functional group is not involved in the adsorption of Cd^{2+}. The adsorption peak at 1,397 cm^{-1} is an adsorption peak with benzene ring framework, suggesting that it contains benzene ring-like substances, but after adsorption, the adsorption peak does not shift significantly, suggesting that the functional group is not involved in the adsorption of Cd^{2+}. Additionally, RS700 also contains CO single bond stretching vibration (1,061 cm^{-1}) and O-Si-O bond bending vibration (1,061 cm^{-1}), but after adsorption, the adsorption peak does not shift significantly, suggesting that these functional groups are not involved in the adsorption of Cd^{2+}.

Based on data shown in Figures 14 and 16, it could be found that the mechanism of single and competitive adsorption is not different among RS300, RS500, and RS700, in which O-H stretching vibration or hydroxyl oxygen, C-H stretching vibration, benzene ring structure, and ionic effect are involved.

3.6.3. Mechanism for Competitive Adsorption of Cu^{2+} by Crop-Residual-Derived Charcoal in Acidic Solution. In order to investigate the mechanism for adsorption of Cu^{2+} by crop-residual-derived charcoal in the acidic solution, the measurements have been performed for the infrared spectrums of RS300, RS500, and RS700 before and after adsorption, in which RS300, RS500, and RS700 are used as the adsorbents, and Cu^{2+} is used as the adsorbed substance, as shown in Figure 17.

As it is shown in Figure 17, RS300 has an adsorption peak at 3,435 cm^{-1}, which is O-H stretching vibration or hydroxyl oxygen, but after adsorption, the adsorption peak does not shift significantly, suggesting that the functional group is not involved in the adsorption of Cu^{2+}. The adsorption peak at 1,619 cm^{-1} is an adsorption peak with benzene ring framework, suggesting that it contains benzene ring-like substances, but after adsorption, the adsorption peak does not shift significantly, suggesting that the functional group is not involved in the adsorption of Cu^{2+}. Additionally, RS300 also contains CO single bond stretching vibration (1,088 cm^{-1}) and O-Si-O bond bending vibration (1,088 cm^{-1}), but after adsorption, the adsorption peak does not shift significantly, suggesting that these functional groups are not involved in the adsorption of Cu^{2+}.

RS500 has an adsorption peak at 3,425 cm^{-1}, which is O-H stretching vibration or hydroxyl oxygen, but after adsorption, the adsorption peak does not shift significantly, suggesting that the functional group is not involved in the adsorption of Cu^{2+}. The adsorption peak at 1,615 cm^{-1} is an adsorption peak with benzene ring framework, suggesting that it contains benzene ring-like substances, but after adsorption, the adsorption peak does not shift significantly, suggesting that the functional group is not involved in the adsorption of Cu^{2+}. Additionally, RS500 also contains CO single bond stretching vibration (1,073 cm^{-1}) and O-Si-O bond bending vibration (1,073 cm^{-1}), but after adsorption, the adsorption peak does not shift significantly, suggesting that these functional groups are not involved in the adsorption of Cu^{2+}.

Similarly, RS700 has an adsorption peak at 3,420 cm^{-1}, which is O-H stretching vibration or hydroxyl oxygen, but after adsorption, the adsorption peak does not shift significantly, suggesting that the functional group is not involved in the adsorption of Cu^{2+}. The adsorption peak of RS700 at 1,638 cm^{-1} is an adsorption peak with benzene ring framework, suggesting that it contains benzene ring-like substances, and after adsorption, the adsorption peak transfers to 1,562 cm^{-1} through red shift, suggesting that a π-π conjugated structure exists among the aromatic structure formed by Cu^{2+} and RS700. Additionally, RS700 also contains CO single bond stretching vibration (1,064 cm^{-1}) and O-Si-O bond bending vibration (1,064 cm^{-1}), but after adsorption, the adsorption peak does not shift significantly, suggesting that these functional groups are not involved in the adsorption of Cu^{2+}.

Based on data shown in Figures 14 and 17, it could be found that the mechanism of single and competitive adsorption is not different among RS300, RS500, and RS700, in which O-H stretching vibration or hydroxyl oxygen, C-H stretching vibration, benzene ring structure, and ionic effect are involved.

3.6.4. Mechanism for Competitive Adsorption of Zn^{2+} by Crop-Residual-Derived Charcoal in Acidic Solution. In order to investigate the mechanism for adsorption of Zn^{2+} by crop-residual-derived charcoal in the acidic solution, the measurements have been performed for the infrared spectrums of RS300, RS500, and RS700 before and after adsorption, in which RS300, RS500, and RS700 are used as the adsorbents, and Zn^{2+} is used as the adsorbed substance, as shown in Figure 18.

As it is shown in Figure 18, RS300 has an adsorption peak at 3,427 cm^{-1}, which is O-H stretching vibration or hydroxyl oxygen, and after adsorption of Zn^{2+}, the adsorption peak transfers to 3,407 cm^{-1} through blue shift. The adsorption peak of RS300 at 2,926 cm^{-1} is C-H stretching vibration, and after adsorption of Zn^{2+}, the adsorption peak transfers to 2,935 cm^{-1} through red shift. It suggests that hydrogen bond structure is formed by Zn^{2+} and RS300. The adsorption peak at 1,631 cm^{-1} is an adsorption peak with benzene ring framework, suggesting that it contains benzene ring-like substances. After adsorption, the adsorption peak transfers to 1,641 cm^{-1} through red shift, suggesting that a π-π conjugated structure exists among the aromatic structure formed by Zn^{2+} and RS300. Additionally, RS300 also contains CO single bond stretching vibration (1,086 cm^{-1}) and O-Si-O band bending vibration (1,086 cm^{-1}), but after adsorption, the adsorption peak does not shift significantly, suggesting that these functional groups are not involved in the adsorption of Zn^{2+}.

RS500 has an adsorption peak at 3,427 cm^{-1}, which is O-H stretching vibration or hydroxyl oxygen, and after adsorption of Zn^{2+}, the adsorption peak transfers to 3,456 cm^{-1} through red shift. The adsorption peak of RS500 at 2,979 cm^{-1} is C-H stretching vibration, and after adsorption of Zn^{2+}, the adsorption peak transfers to 2,930 cm^{-1} through blue shift. It suggests that hydrogen bond structure is formed by Zn^{2+} and RS500. The adsorption peak at 1,641 cm^{-1} is an adsorption peak with benzene ring framework, suggesting that it contains benzene ring-like substances. After adsorption, the adsorption peak transfers to 1,619 cm^{-1} through red shift, suggesting that a π-π conjugated structure exists among the aromatic structure formed by Zn^{2+} and RS500. Additionally, RS500 also contains CO single bond stretching vibration (1,066 cm^{-1}) and O-Si-O band bending vibration (1,066 cm^{-1}), but after adsorption, the adsorption peak does not shift significantly, suggesting that these functional groups are not involved in the adsorption of Zn^{2+}.

Similarly, RS700 has an adsorption peak at 3,412 cm^{-1}, which is O-H stretching vibration or hydroxyl oxygen, and after adsorption of Zn^{2+}, the adsorption peak transfers to 3,432 cm^{-1} through blue shift. The adsorption peak of RS700 at 2,926 cm^{-1} is C-H stretching vibration, but after adsorption, the adsorption peak does not shift significantly, suggesting that the functional group is not involved in the adsorption of Zn^{2+}. The adsorption peak at 1,626 cm^{-1} is an adsorption peak with benzene ring framework, suggesting that it contains benzene ring-like substances, but after adsorption, the adsorption peak does not shift significantly, suggesting that the functional group is not involved in the adsorption of Zn^{2+}. Additionally, RS700 also contains CO single bond stretching vibration (1,105 cm^{-1}) and O-Si-O band bending vibration (1,105 cm^{-1}), but after adsorption, the adsorption peak does not shift significantly, suggesting that these functional groups are not involved in the adsorption of Zn^{2+}.

Based on data shown in Figures 14 and 18, it could be found that the mechanism of single and competitive adsorption is not different among RS300, RS500, and RS700, in which O-H stretching vibration or hydroxyl oxygen, C-H stretching vibration, benzene ring structure, and ionic effect are involved.

4. Discuss

(1) The crop-residual-derived charcoal produced at different temperatures could form different effects on the adsorption of four heavy metal ions, i.e., Pb^{2+}, Cd^{2+}, Cu^{2+}, and Zn^{2+}, and the adsorption capacity of charcoal is not affected significantly by the concentration of heavy metal ions. The result of the experiment shows that the crop-residual-derived charcoal produced at 300°C is most effective in adsorbing Pb^{2+}; the crop-residual-derived charcoal produced at 500°C is most effective in adsorbing Cd^{2+}, and the crop-residual-derived charcoal produced at 700°C is most effective in adsorbing Cu^{2+}

(2) The crop-residual-derived charcoal is most ineffective in adsorbing Zn^{2+}, though when the concentration is 2.000 mmol/L, the competitive adsorption rate reaches the maximum level, i.e., 25.0%, 50.0%, and 73.5%, respectively, and when the concentration is 0.5000 mmol/L, the adsorption amount could reach 21.36 mmol/kg. However, the adsorption amount is not large, and when the concentration is 1.000 mmol/L or higher, the adsorption amount becomes zero. Meanwhile, during desorption, the desorption rate decreases to zero as the concentration of Zn^{2+} increases. It suggests that a high concentration of Zn^{2+} is maintained in the crop-residual-derived charcoal, so it is not suitable to adsorb such a heavy metal ion

(3) The crop-residual-derived charcoal shows a better adsorption effect to Pb^{2+} in the acidic mixed heavy metal solution, comparing with the other three heavy metal ions, i.e., Cd^{2+}, Cu^{2+}, and Zn^{2+}, and the adsorption amount could reach 410.20 mmol/kg, with an adsorption rate of 65% ~75%. The competitive desorption rate keeps unchanged as the concentration of Pb^{2+} increases, and it could reach a level as low as 5.35%. It suggests that the adsorption of Pb^{2+} by the crop-residual-derived charcoal is very stable in the acidic solution, and the heavy metal ion could not be desorbed easily

(4) Competitive adsorption of Pb^{2+}, Cd^{2+}, Cu^{2+}, and Zn^{2+} by all three types of the crop-residual-derived charcoal (i.e., RS300, RS500, and RS700) in the acidic solution shows a good fit to the isothermal equation

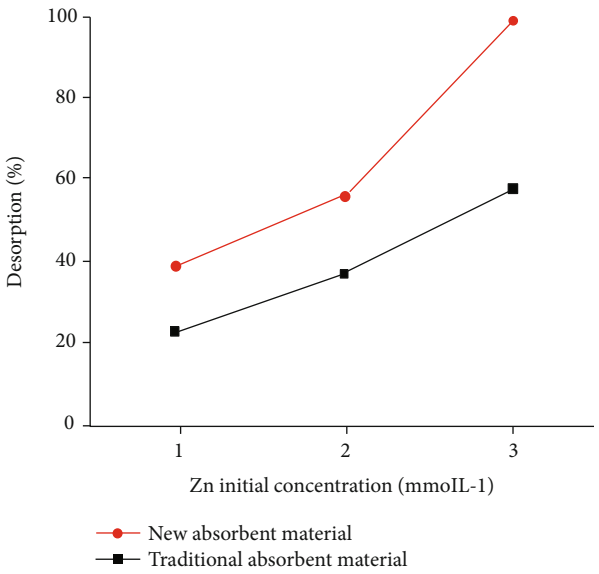

Figure 19: Adsorption of Pb ions by new adsorbent materials and traditional adsorbent materials.

of Freundlich model, in which R^2 values are all more than 0.9. It suggests that the competitive adsorption and desorption of Pb^{2+}, Cd^{2+}, Cu^{2+}, and Zn^{2+} by the crop-residual-derived charcoal are all in the standard Freundlich adsorption mode

(5) All three types of the crop-residual-derived charcoal (i.e., RS300, RS500, and RS700) have O-H stretching vibration or hydroxyl oxygen and adsorption peak of benzene framework. The charcoal adsorbs the heavy metal ions (Pb^{2+}, Cd^{2+}, Cu^{2+}, and Zn^{2+}) in the mechanism that the surface hydroxylated functional group of the charcoal combines with the heavy metal ion to form a hydrogen bond, and the aromatic structure of the charcoal combines with the heavy metal ion to form a π-π coagulated structure

5. Comparison of New Adsorbent Materials with Traditional Adsorbent Materials

This paper is designed to investigate the competitive adsorption and desorption of Pb^{2+}, Cd^{2+}, Cu^{2+}, and Zn^{2+} by the crop-residual-derived charcoal in the acidic solution and their mechanism through the static adsorption test in which three crop-residual-derived charcoal products, identified as RS300, RS500, and RS700, are made from the crop residual, respectively, at 300°C, 500°C, and 700°C with the low-temperature pyrolysis technology. The result shows that RS300 is the most effective product in adsorbing Pb^{2+} in the acidic solution, RS500 is the most effective one in adsorbing Cd^{2+} in the acidic solution, and RS700 is the most effective one in adsorbing Cu^{2+} in the acidic solution, and that the competitive adsorption and desorption of Pb^{2+}, Cd^{2+}, Cu^{2+}, and Zn^{2+} by the crop-residual-derived charcoal in the acidic solution are related to the concentrations of these heavy metal ions. However, the fluctuation of adsorption and desorption is relatively small as the concentrations of heavy metal ions increase.

The adsorption effect of the new adsorbent materials was studied. Compared with the adsorption effect of the conventional adsorbent materials on Pb2+ under RS300, RS500, and RS700, it can be seen from Figure 19 that the effect of adsorption increases with the increase of temperature. The adsorption effect of biochar is better, and it is found that biochar can be used as a new type of adsorbent material, which has a much stronger adsorption effect than conventional adsorbent materials.

6. Conclusion

This paper studies that the competitive adsorption and desorption are not significantly affected by the concentration of heavy metal ions. The mechanism of single and competitive adsorption is not different among RS300, RS500, and RS700, in which O-H stretching vibration or hydroxyl oxygen, C-H stretching vibration, benzene ring structure, and ionic effect are involved, and it is an advantage for the charcoal as a new adsorption material; the adsorption effect of biochar on heavy metal ions has a distinct advantage over traditional adsorbent materials, and biochar is a renewable energy source, which is cheap and better for recycling resources.

Data Availability

The experimental data used to support the findings of this study are included within the article.

Conflicts of Interest

The authors declare that there are no conflicts of interest regarding the publication of this paper.

Acknowledgments

This paper was supported by the National Natural Science Foundation of China (No. 51808510).

References

[1] H. Hu, Q. Jin, and P. Kavan, "A study of heavy metal pollution in China: Current status, pollution-control policies and countermeasures," *Sustainability*, vol. 6, no. 9, pp. 5820–5838, 2014.

[2] J. Meng, *Change of Heavy Metal Fractions during the Composting and Pyrolysis Processes of Swine Manure and the Applications of Its Composts and Biochars*, Zhengjiang University, 2014.

[3] ICoEP Department, *Macro Strategic Study on China's Environment*, China Agricultural Science and Technology Press, 2011.

[4] Y. Luo, "Soil environmental problems and solutions in China," *Hohai University Press*, vol. 19, no. 6, pp. 356–359, 2008.

[5] J. Xu, *The Heavy Metal in Terrestrial Ecosystems*, China Environmental Science Press, 1995.

[6] S. Jiang, C. Lu, S. Zhang et al., "Prediction of ecological pressure on resource-based cities based on an RBF neural network

optimized by an improved ABC algorithm," *IEEE Access*, vol. 7, pp. 47423–47436, 2019.

[7] H. Lu, G. Xiao, Q. Liu, and X. Peng, "Advances in soil cd pollution and solution measures," *Journal of Southern Agriculture*, vol. 45, pp. 1986–1993, 2014.

[8] Q. Gu, S. Jiang, M. Lian, and C. Lu, "Health and safety situation awareness model and emergency management based on multi-sensor signal fusion," *IEEE Access*, vol. 2019, no. 7, pp. 958–968, 2007.

[9] Y. Li, *Environmental Problems and Countermeasures of Intensive Agriculture*, China Agricultural Science and Technology Press, 2001.

[10] B. Song, D. Gao, T. Chen et al., "A survey of chromium concentrations in vegetables and soils in Beijing and the potential risks to human health," *Acta Scientiae Circumstantiae*, vol. 26, pp. 1343–1353, 2006.

[11] F. J. Ai, X. Z. Yin, R. C. Hu, H. L. Ma, and W. Liu, "Research into the super-absorbent polymers on agricultural water," *Agricultural Water Management*, vol. 245, article 106513, 2021.

[12] W. Liu, H. L. Ma, and A. Walsh, "Advance in photonic crystal solar cells," *Renewable and Sustainable Energy Reviews*, vol. 116, article 109436, 2019.

[13] P. K. Malik, "Use of activated carbons prepared from sawdust and rice-husk for adsorption of acid dyes: a case study of Acid Yellow 36," *Dyes and Pigments*, vol. 56, no. 3, pp. 239–249, 2003.

[14] X. Zhang, C. Zang, H. L. Ma, and Z. J. Wang, "Study on removing calcium carbonate plug from near wellbore by high-power ultrasonic treatment," *Ultrasonics Sonochemistry*, vol. 62, article 104515, 2020.

[15] H. L. Ma, X. Zhang, F. F. Ju, and S. B. Tsai, "A study on curing kinetics of nano-phase modified epoxy resin," *Scientific Reports*, vol. 8, no. 1, p. 3045, 2018.

[16] M. Ling, M. J. Esfahani, H. Akbari, and A. Foroughi, "Effects of residence time and heating rate on gasification of petroleum residue," *Petroleum Science and Technology*, vol. 34, no. 22, pp. 1837–1840, 2016.

[17] H. L. Ma and S. B. Tsai, "Design of research on performance of a new iridium coordination compound for the detection of Hg^{2+}," *International Journal of Environmental Research and Public Health*, vol. 14, no. 10, p. 1232, 2017.

[18] L. Y. Mo, W. H. Z. Sun, S. Jiang et al., "Removal of colloidal precipitation plugging with high-power ultrasound," *Ultrasonics Sonochemistry*, vol. 69, article 105259, 2020.

[19] D. Gao, Y. Liu, Z. Guo et al., "A study on optimization of CBM water drainage by well-test deconvolution in the early development stage," *Water*, vol. 10, no. 7, p. 929, 2018.

[20] S. B. Tsai and H. Ma, "A research on preparation and application of the monolithic catalyst with interconnecting pore structure," *Scientific Reports*, vol. 8, no. 1, article 16605, 2018.

[21] X. Jiang, A. Lin, H. Ma, X. Li, and Y. Li, "Minimizing the thermal bridge through the columns in a refrigeration room," *Applied Thermal Engineering*, vol. 165, article 114565, 2020.

[22] W. Liu, H. Shi, H. Ma, and S. Tsai, "Improving renewable energy source in automotive applications: evaluation, analysis, and design," in *Green Production Strategies for Sustainability*, S. Tsai, B. Liu, and Y. Li, Eds., pp. 210–237, IGI Global, 2018.

[23] J. Xie and H. Ma, "Application of improved APO algorithm in vulnerability assessment and reconstruction of microgrid," *IOP Conference Series: Earth and Environmental Science*, vol. 108, no. 5, article 052109, 2018.

[24] H. Ma, "Experimental study on simultaneous desulfurization and denitrification of doped Tio2 based on photocatalysis," *Acta Chemica Malaysia*, vol. 1, 2017.

[25] B. S. Girgis, S. S. Yunis, and A. M. Soliman, "Characteristics of activated carbon from peanut hulls in relation to conditions of preparation," *Materials Letters*, vol. 57, no. 1, pp. 164–172, 2002.

[26] D. Xu and H. Ma, "Degradation of rhodamine B in water by ultrasound-assisted TiO_2 photocatalysis," *Journal of Cleaner Production*, vol. 313, p. 127758, 2021.

[27] S. M. Yakout and G. Sharaf el-Deen, "Characterization of activated carbon prepared by phosphoric acid activation of olive stones," *Arabian Journal of Chemistry*, vol. 9, pp. S1155–S1162, 2016.

[28] J. Jaramillo, V. Gómez-Serrano, and P. M. Álvarez, "Enhanced adsorption of metal ions onto functionalized granular activated carbons prepared from cherry stones," *Journal of Hazardous Materials*, vol. 161, no. 2-3, pp. 670–676, 2009.

[29] J. M. Rosas, J. Bedia, J. Rodríguez-Mirasol, and T. Cordero, "On the preparation and characterization of chars and activated carbons from orange skin," *Fuel Processing Technology*, vol. 91, no. 10, pp. 1345–1354, 2010.

[30] L. C. A. Oliveira, E. Pereira, I. R. Guimaraes et al., "Preparation of activated carbons from coffee husks utilizing FeCl3 and ZnCl2 as activating agents," *Journal of Hazardous Materials*, vol. 165, no. 1-3, pp. 87–94, 2009.

[31] M. Fan, "Steam activation of chars produced from oat hulls and corn stover," *Bioresource Technology*, vol. 93, no. 1, pp. 103–107, 2004.

[32] Y. Sudaryanto, S. B. Hartono, W. Irawaty, H. Hindarso, and S. Ismadji, "High surface area activated carbon prepared from cassava peel by chemical activation," *BioresourceTechnol.*, vol. 97, no. 5, pp. 734–739, 2006.

[33] Q. Lin, *Experimental Study on Cu, Cd, Zn, Pb Adsorption and Migration of Heavy Metals in Soil*, Qingdao University, 2008.

[34] M. Jalali and F. Moradi, "Competitive sorption of Cd, Cu, Mn, Ni, Pb and Zn in polluted and unpolluted calcareous soils," *Environmental Monitoring and Assessment*, vol. 185, no. 11, pp. 8831–8846, 2013.

[35] Y. Wang, *Determination of Different Forms of Zinc/Cadmium and Chromium by Flame Atomic Absorption Spectrometry after Liquid-Liquid Extraction, in*, Zhengzhou University, 2012.

[36] H. Li, L. Luo, P. Kunal et al., "Oxygen reduction reaction on classically immiscible bimetallics: a case study of RhAu," *The Journal of Physical Chemistry C*, vol. 122, no. 5, pp. 2712–2716, 2018.

[37] H. Li and G. A. Henkelman, "Dehydrogenation selectivity of ethanol on close-packed transition metal surfaces: a computational study of monometallic, Pd/Au, and Rh/Au catalysts," *The Journal of Physical Chemistry C*, vol. 121, no. 49, pp. 27504–27510, 2017.

[38] H. Zhao, X. Mu, C. Zheng et al., "Structural defects in 2D MoS_2 nanosheets and their roles in the adsorption of airborne elemental mercury," *Journal of Hazardous Materials*, vol. 366, pp. 240–249, 2019.